

# STUDY OF BUOYANCY EFFECTS ON A THERMAL MIXING LAYER USING AN X-WIRE PROBE OPERATED SEQUENTIALLY AT DIFFERENT OVERHEATS

**Kodjovi Sodjavi**

Irstea, Université Européenne de Bretagne, F-35044 Rennes, France  
kodjovi.sodjavi@gmail.com

**Johan Carlier**

Irstea, Université Européenne de Bretagne, F-35044 Rennes, France  
johan.carlier@irstea.fr

## ABSTRACT

The turbulent mixing was studied in a thermal plane turbulent mixing layer induced by two parallel and horizontal incident streams with velocity and temperature differences. The instantaneous velocity and temperature fluctuations in the mixing layer were measured using variable temperature hot wire thermo-anemometry with an  $\times$ -wire probe. A particular attention was paid to the effect of buoyancy forces on two counter-gradient configurations so-called stable and unstable, in relation to the sign of the vertical temperature gradient applied. The buoyancy effects were discussed in terms of transport equations of turbulent kinetic energy and temperature variance. In view of the low Richardson values at stake ( $Ri_f < 0.03$ ) the buoyancy forces appeared logically to be quantitatively negligible compared to the main driving forces, but such a low energy forcing mechanism was in fact sufficient in the unstable configuration to increase significantly the shear stress and the expansion rate of the mixing layer, both phenomena being associated with enhanced production of turbulence. In addition, joint probability density function analysis highlighted the mechanisms and events that significantly contribute to the transverse momentum and heat fluxes. These contributions were differentiated and quantified through quadrant analysis which emphasized the dominance of the local movements of entrainment and ejection, their dissymmetries and the effects of buoyancy.

## 1 Introduction

The air flows in industrial devices for separating climatic environments are in many ways analogous to the thermal mixing layer flow, especially when the mean velocity and temperature profiles are in counter-gradient (the high speed flow on one side is cold and the low speed flow on the other side is hot). The present study focused specifically on the momentum and heat fluxes across the thermal mixing layer, responsible of the mixing between the two environments. If the mixing layer is a relatively well-documented academic flow for the kinematic and heat behaviors considered separately, the velocity and temperature coupling remains poorly understood. The difficulty lies in the instantaneous measuring of velocity and temperature in a small

volume and at high frequency. The variable temperature hot wire thermo-anemometry is a measurement method that meets these requirements. The method was recently developed by Ndoye (2008) for simultaneous measurement of temperature and only the longitudinal component of the velocity, by using a single wire probe. The method was extended by Sodjavi (2013) to use an  $\times$ -wire probe and then to measure in addition the transverse component of the velocity, responsible of the transport through the mixing layer.

The method proposed by Sodjavi was used to explore thermal mixing layer in two counter-gradient configurations so-called stable and unstable, in relation to the sign of the vertical temperature gradient applied. The influence of the buoyancy on the flow was discussed in terms of transport equations of turbulent kinetic energy and temperature variance. Joint probability density function of velocity and temperature through the mixing layer in the self-similar region was assessed to highlight the mechanisms and events that significantly contribute to the transverse momentum and heat fluxes. These contributions were differentiated and quantified through quadrant analysis.

## 2 Experiments

We describe briefly in this section the wind tunnel dedicated to the study of the mixing layer, the variable temperature hot wire thermo-anemometry method and the explored flow configurations. Further details can be found in Ndoye (2008) and Sodjavi (2013).

### 2.1 Wind tunnel

The wind tunnel is equipped with two juxtaposed open circuits. Two parallel air streams are blown separately through two independent halves of a conditioning chamber comprising several screens and a convergent entrance cone with a contraction coefficient of 2.5. The two streams are separated by a thick thermal insulating plate with a tapering angle at the trailing edge of about  $3^\circ$ . These two streams merge and initiate the mixing process downstream from the trailing edge of the splitter plate. The test section of the tunnel is  $1 \times 1 \text{ m}^2$  and the length is 3 m. Downstream from the test section, the mixed flow is evacuated through a diver-

gent exit cone. The origin of the coordinate system  $(x, y, z)$  is located at the center of the trailing edge of the separating plate. The longitudinal streamwise direction provides the  $x$  axis, the upward transverse direction the  $y$  axis and the spanwise direction of the mixing layer the  $z$  axis. The velocity and temperature profiles are uniform at the entrance of the test section. The velocity and temperature can be chosen continuously and independently, from 0.5 to 5 m/s and from 5 to 35 °C, respectively. The turbulence levels are lower than 1% for velocity and 0.2 °C for temperature in the free stream outside the boundary and the mixing layers. The boundary layers over the separating plates are tripped downstream to establish the turbulence state and the onset of the transition. The momentum thickness of the boundary layer is about 2 mm with a shape factor of around 1.4, as expected for the turbulence state.

## 2.2 Variable temperature hot wire thermo-anemometry

The multiple overheat thermo-anemometry was initially proposed by Corrsin (1947). Assuming hot wire is sensitive to velocity for high overheat and to temperature for low overheat, the effects of velocity and temperature can be separated by using hot wire subjected to different overheats. The overheats may be applied either simultaneously to different wires or sequentially to a single or several wires. The second method has the advantage of minimizing the number of wire, and therefore to reduce the measurement volume and to avoid interference problems, at the expense of strictly instantaneous measurements. This method was implemented in a variable temperature hot wire thermo-anemometer invented by Joël Delville (from Pprime Institute). Several overheat steps are applied cyclically so that the wire changes suddenly from a constant temperature step to another. The instantaneous velocity and temperature of the flow, assumed to be constant along of a short cycle, are deduced from the resolution of a previously calibrated system linking the velocity and the temperature to the voltages of the different overheat steps. In the present study,  $\times$ -wire probe with wire diameter of 2.5  $\mu\text{m}$  and wire length of 0.8 mm associated with two overheat steps by 1 ms cycle enabled an acquisition frequency of 1 kHz.

## 2.3 Configurations

A flow configuration is defined by the convection velocity  $U_c = \frac{U_h + U_l}{2}$ , the velocity difference between the two parallel flows  $\Delta U = U_h - U_l$  (or the modified velocity ratio  $\lambda = \frac{\Delta U}{2U_c}$ ) and the temperature difference  $\Delta\Theta = \Theta_h - \Theta_l$ . The subscripts  $h$  and  $l$  correspond to the high and low free stream velocity or temperature, respectively. In addition to these parameters, it is necessary to specify whether the mean velocity and temperature profiles are in co- or counter-gradient, and if the “forced” temperature stratification (the mixing layer is horizontal) is stable or unstable against buoyancy. In this study, analysis of the results was based on three mixing layer configurations with  $\lambda = 0.33$  and  $U_c = 3$  m/s, one isothermal configuration with  $\Delta\Theta = 0$  K and two counter-gradient configurations with  $\Delta\Theta = 20$  K, one stable and the other unstable. The measurement grid was 911 points distributed along 11 transverse profiles. The acquisition frequency of 1 kHz and the acquisition time of 60 s were sufficient to resolve scales of the turbulent flow and to ensure the convergence of second and third order moment at each point of the grid.

## 3 Results and discussion

It is well known that turbulent mixing layer evolves self-similarly, with geometrical affinity of statistical quantity profiles and linearly increasing thickness. For all the configurations explored the self-similar region began at about 1 000 mm downstream of the trailing edge, equivalent to 800 momentum thicknesses of the boundary layer on the high-velocity side. In this section, the results are given in the self-similar region and are therefore represented using the similarity variable  $\eta_{u,\theta} = \frac{y-y_0}{\delta_{u,\theta}}$ , where  $\delta_{u,\theta}$  is the kinematic (subscript  $u$ ) or thermal (subscript  $\theta$ ) thickness of the mixing layer, and  $y_0$  is the axis of the mixing layer.

### 3.1 Moments

The mean and turbulence properties in the self-similar region of the stable configuration are shown in Figure 1. The profiles are given for the average temperature and velocity, variances of the fluctuations, momentum and heat fluxes involved in the turbulent production, and triple correlations involved in the turbulent diffusion. The mean longitudinal velocity profile is symmetrical with one single inflection point located on the axis of the mixing layer. In contrast, the mean temperature profile has three inflection points. This typical behavior is stressed in numerous studies (see Fiedler (1974) for exemple). The location of the inflection points coincide with the velocity and temperature variance extrema. The peak of  $\langle u'u' \rangle$  is centered and corresponds to the maximum production of turbulent kinetic energy ( $\langle u'v' \rangle \frac{\partial \langle u \rangle}{\partial y}$ ). The peak of  $\langle v'v' \rangle$  is slightly shifted toward the low velocity side, as reported by Wignanski & Fiedler (1970). The double peak of  $\langle \theta'\theta' \rangle$  on both sides of the axis is not symmetrical, the largest peak being on the low velocity side. This double peak is associated with the two largest extrema of the mean temperature gradient and corresponds to a maximum production of temperature fluctuations ( $\langle v'\theta' \rangle \frac{\partial \langle \theta \rangle}{\partial y}$ ).

The shapes of the isothermal and unstable configuration profiles (not shown) are nearly identical. The differences due to buoyancy forces can be summarized in terms of expansion rates and turbulence levels. For the isothermal and stable configurations, these values are approximately the same. The kinematic and thermal expansion rates are 0.055 and 0.074, respectively, and the maximum shear stress is  $0.012\Delta U^2$ . For the unstable configuration, these values increase. The kinematic and thermal expansion rate are 0.067 and 0.090, respectively, and the maximum shear stress is  $0.019\Delta U^2$ . The kinematic and thermal expansion rates increases in the same proportion, so that the ratio remains at 0.74, close to the value of 0.72 obtained by Batt (1977), but the turbulence level increases in more significant proportions.

In view of the low Richardson values at stake ( $Ri_f < 0.03$ ) in this study, the buoyancy forces appeared to be quantitatively negligible compared to the main driving forces. However, such a low energy forcing mechanism was in fact sufficient in the unstable configuration to increase significantly the shear stress and the expansion rate of the mixing layer with a fluctuating flow (shear stress) more sensitive than the mean flow (expansion rate). The dissymmetric effects observed between stable and unstable configurations suggest that the forcing mechanism is mostly effective when it destabilizes the flow.

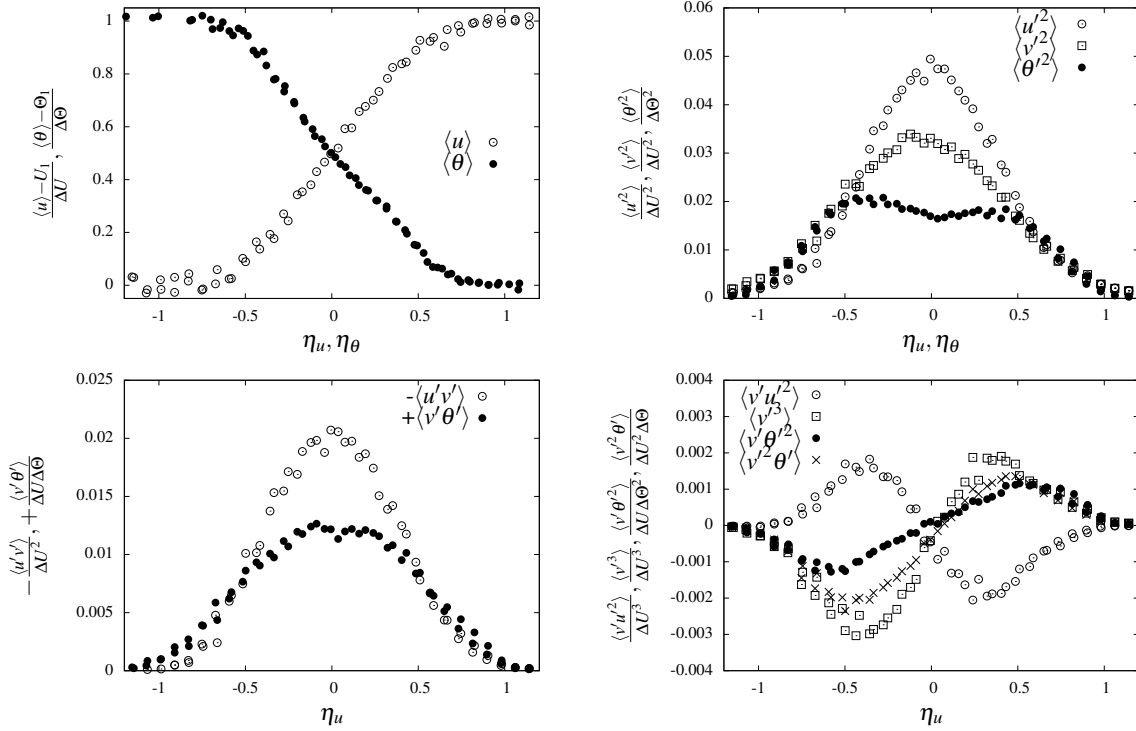


Figure 1. Transverse profiles in the self-similar region for the stable configuration.

### 3.2 Balance equations

Temperature gradient effects on the mixing layer can be studied using various terms of the transport equation, which have more physical significance. For the thermal mixing layer, the transport equations of turbulent kinetic energy and temperature variance can be derived under the boundary layer and Boussinesq approximations, assuming they are steady, taking into account the self-similarity of the flow and dropping the viscous and molecular diffusion terms. These transport equations can be normalized using the differences in free stream velocity and temperature ( $\Delta U, \Delta \Theta$ ), the high free stream velocity and temperature ( $U_h, \Theta_h$ ) and the thickness of the mean velocity and temperature profiles ( $\delta_u, \delta_\theta$ ).

These equations contain the terms which are identified according to their roles. The condensed form can be written as:

$$C + P + Dfu + Dfp + Ds + B = 0, \quad (1)$$

where  $C$  = Convection;  $P$  = Production;  $Dfu$  = Turbulent diffusion by the velocity fluctuations;  $Dfp$  = Turbulent diffusion by the pressure fluctuations;  $Ds$  = Dissipation;  $B$  = Buoyancy.

For the turbulent kinetic energy equation, normalized by  $\left[\frac{U_h \Delta U^2}{\delta_u}\right]$ , these terms can be written as:

$$\begin{aligned} C &= \left[ \frac{\langle v \rangle}{U_h} - \eta_u \frac{d\delta_u \langle u \rangle}{dx U_h} \right] \frac{d}{d\eta_u} \left( \frac{\langle k' \rangle}{\Delta U^2} \right), \\ P &= \frac{\langle u'v' \rangle}{\Delta U^2} \frac{d}{d\eta_u} \left( \frac{\langle u \rangle}{U_h} \right), \\ Dfu &= (1 - r_u) \frac{d}{d\eta_u} \left( \frac{\langle k'v' \rangle}{\Delta U^3} \right), \end{aligned}$$

$$\begin{aligned} Dfp &= (1 - r_u) \frac{d}{d\eta_u} \left( \frac{\langle p'v' \rangle}{\rho_0 \Delta U^3} \right), \\ Ds &= \frac{\delta_u \nu}{U_h \Delta U^2} \langle (\frac{\partial u'_i}{\partial x_i})^2 \rangle, \\ B &= - \frac{\delta_u g}{U_h \Delta U} \frac{\langle v'\theta' \rangle}{\Delta U \langle \theta \rangle}. \end{aligned}$$

Similarly, for the temperature fluctuation equation normalized by  $\left[\frac{U_h \Delta \Theta^2}{\delta_\theta}\right]$ , the terms  $Dfp$  and  $B$  are not present and the others can be written as:

$$\begin{aligned} C &= \left[ \frac{\langle v \rangle}{U_h} - \eta_\theta \frac{d\delta_\theta \langle u \rangle}{dx U_h} \right] \frac{d}{d\eta_\theta} \left( \frac{\langle \frac{1}{2} \theta'^2 \rangle}{\Delta \Theta^2} \right), \\ P &= - \frac{(1 - r_u) \langle v'\theta' \rangle}{(1 - r_\theta) \Delta U \Delta \Theta} \frac{d}{d\eta_\theta} \left( \frac{\langle \theta \rangle}{\Theta_h} \right), \\ Dfu &= -(1 - r_u) \frac{d}{d\eta_\theta} \left( \frac{\langle \frac{1}{2} v'\theta'^2 \rangle}{\Delta U \Delta \Theta^2} \right), \\ Ds &= - \frac{\delta_\theta \kappa}{U_h \Delta \Theta^2} \langle (\frac{\partial \theta'_i}{\partial x_i})^2 \rangle. \end{aligned}$$

In these equations,  $\nu$  is the kinematic viscosity,  $k$  the thermal diffusivity,  $\rho_0$  the mean density and  $g$  the acceleration due to gravity.

Figure 2 summarizes the transverse profiles of all the different terms in turbulent kinetic energy and temperature fluctuation balance equations. These profiles are given for stable and unstable configurations in the self-similar region.

The two budgets reveal certain constants in behavior of different terms. The production and dissipation terms are found to dominate the budgets along with turbulent diffusion by velocity. The first term has the role of a source and

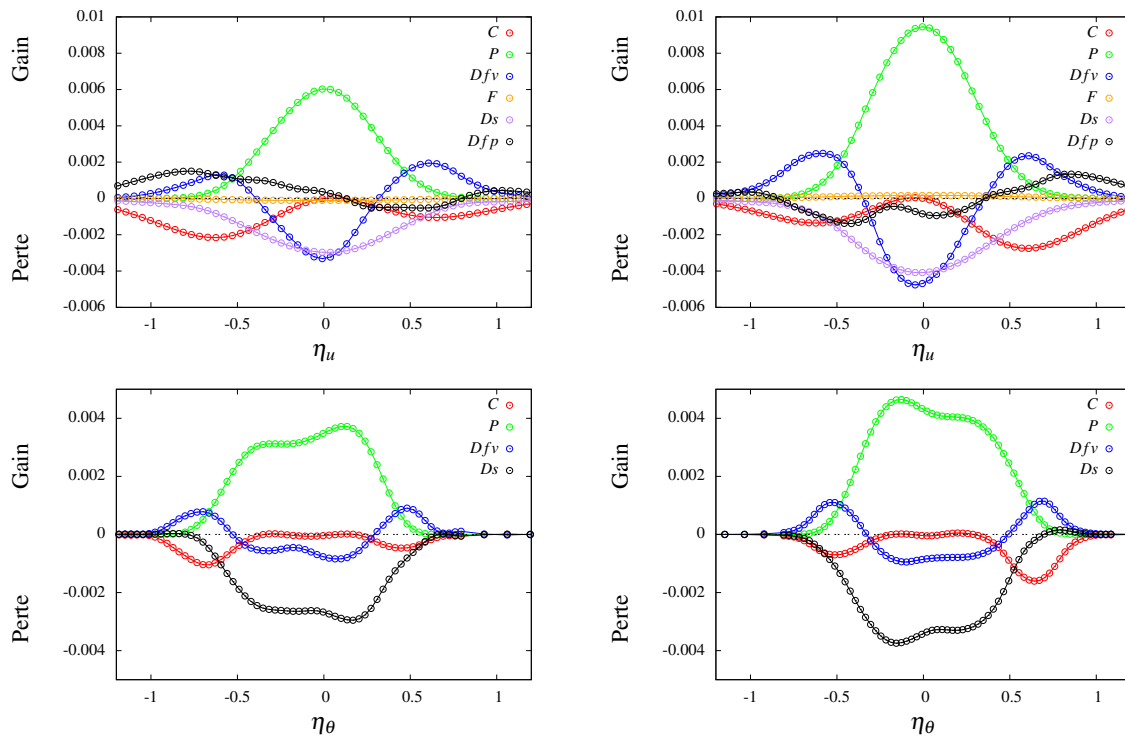


Figure 2. Top, turbulent kinetic energy balance; Bottom, temperature fluctuation balance; Left, stable configuration; Right, unstable configurations

the second term a sink across the flow, whereas the third term acts both as a sink in the center of mixing and as a source at the outer edges.

The peak of production for turbulent kinetic energy is centered on the mixing layer axis and coincides with the inflection point of the mean velocity profile, as explained above. Similarly, for temperature fluctuations, the production term has two peaks whose positions correspond approximately to the two inflection points of the highest gradients on the mean temperature profile. The dissipation term shows a similar but reversed shape, confirming that high production is almost compensated for by high dissipation. The convection term in both budgets is zero at the center of the mixing layer and negative at the outer edges, and it reflects the energy subtracted from the mean flow. It is maximal on the high velocity side. This dissymmetry between the high and low velocity sides is typical for the mixing layer and reveals that the mixing region is fed mainly by the high velocity stream.

The excess heat or energy production resulting from the sum of dissipation and production at the center of the mixing layer is transported by the turbulent diffusion process (negative sign) outwards (positive sign) where it is balanced mainly by convection and partly by dissipation. The turbulent diffusion by the pressure that was inferred also has a redistribution role. It acts as a gain term on the high velocity side and a loss term on the low velocity side. It is the only term with a nearly even shape, and this seems to express the slight dissymmetry in the other terms. The two diffusion terms integrate to approximately zero across the mixing layer as required.

With a low or even quantitatively negligible contribution to the balance, the buoyancy appears to be a loss term for the stable configuration and a gain term for the unsta-

ble configuration. In the unstable configuration, it becomes a driving mechanism, which injects energy into the flow. This low energy injection is in fact sufficient to destabilize the flow and to increase the shear stress significantly and the rate of expansion of the mixing layer to a lesser extent. This mechanism is highlighted by comparing the budgets of turbulent kinetic energy in two stability configurations. In particular, the buoyancy effects are more pronounced for production along with the turbulent diffusion process. For the temperature variance budget all the terms in the unstable configuration increase in the same proportion as the thermal expansion rate, suggesting no change in the equilibrium between the different mechanisms. Thus only the thermal expansion rate is sufficient to express global buoyancy effects on both the mean and fluctuating temperature fields.

### 3.3 Joint Probability Density Functions

Figure 3 presents the evolution of Joint Probability Density Functions  $P_{u',v'}$  and  $P_{v',\theta'}$  through the mixing layer in the self-similar region for the stable configuration. These JPDFs can be analyzed by considering the coherent structures of the flow, and their relationships. In addition to the classical eddy structures commonly identified in the literature, we introduce two additional events, the entrainment and ejection movements, for their significant contributions to the momentum and heat transverse fluxes and to the production of turbulence. Figure 4 illustrates our view on the turbulent mixing layer topology largely based on the literature. The spatio-temporal organization of the flow consists of succession of large eddies with intermittent pairing mechanism. The core of the large eddies constitute regions of turbulence and are responsible of the entrainment and ejection movements around. Entrainment movements are

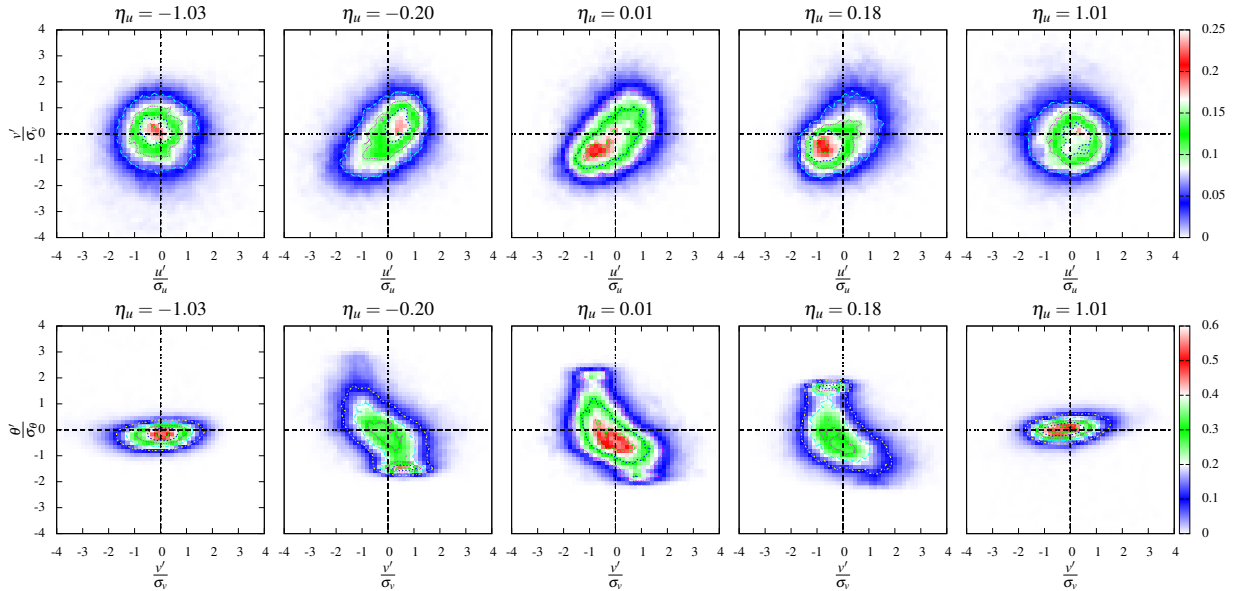


Figure 3. JPDFs associated to the distributions of  $(v', u')$  and  $(v', \theta')$  through the mixing layer in the self-similar region for the stable configuration.

fluid continuously drawn from uniform flow on one or the other side of the mixing layer and become ejection movements when its go through the axis of the mixing layer. We use the terms of mixing regions to name regions of turbulence in the core of the eddies, potential flow ( $\nabla \cdot u = 0$  and  $\nabla \times u = 0$ ) for flow outside of the mixing layer, and front for the high shear at the interface of two potential flow, the shear being located between two large eddies and aligned with the divergent axis of the saddle point. Ejection and entrainment are not the only events that contribute to momentum and heat fluxes. The mixing region and front in the less extend also contribute.

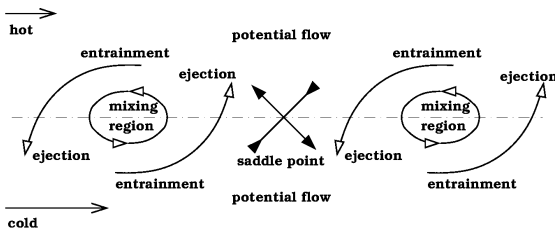


Figure 4. Schematic representation of the turbulent mixing layer topology.

The JPDFs shown in Figure 3 can be divided into four quadrants identified by their number:  $\frac{II}{III} | \frac{I}{IV}$ . Near the border of the mixing layer ( $\eta_u \simeq \pm 1$ ), the JPDFs  $P_{u'v'}$  have a circular shape centered on the origin while the JPDFs  $P_{v'\theta'}$  have an elliptical shape with major axis aligned with  $\theta'$ . This can be explained by a larger expansion rate for the temperature than for the velocity. A circular  $P_{u'v'}$  corresponds to the free flow where PDFs of  $u'$  and  $v'$  are Gaussian. An elliptical  $P_{v'\theta'}$  corresponds to measurement inside the thermal mixing layer where PDFs of  $\theta'$  are non-Gaussian with a high-flatteness factor. Inside the mixing layer ( $-0.25 \leq \eta_u \leq +0.25$ ), the JPDFs  $P_{u'v'}$  have an elliptical shape with a major axis oriented along the quadrants I and III for the stable configuration (and the quadrants II

and IV for the unstable configuration, corresponding Figures not shown). The privileged orientations and the sign of the mean velocity gradient is always consistent with a positive production term in the balance equation. These quadrants are representative of entrainment and ejection events. On either side of the axis of the mixing layer, the elliptical shape, slightly stretched in one of the two quadrants, corresponds to ejections rarer and stronger than entrainments. On the axis of the mixing layer, the two events seem to be balanced approximately.

This analysis of the behavior of JPDFs  $P_{u'v'}$  within the mixing layer can be made identically for  $P_{v'\theta'}$ . We simply note that JPDFs  $P_{v'\theta'}$  has a bimodal shape that breaks the elliptical shape. The central mode corresponds to mixing region and the peripheral mode is located in the quadrant of the entrainment events. Ejections, which appear in the opposite quadrant, again appear rarer and stronger.

The flow in the self-similar region appear as the succession of events with a long and low entrainment, a short and strong ejection and an eddy structure, and so on. Entrainment and ejection on one side of the mixing layer are opposite movements with different temperatures, and are separated by a front. This situation is generator of strong intermittency and variance for temperature fluctuations. Moreover, considering the temperature as a marker of the origin of a fluid particle, the JPDFs  $P_{v'\theta'}$  indicate that the mixing regions in the eddy core are colder than the local mean temperature. This confirms the results of the literature on stronger ejections from the high velocity side, identified by a low temperature.

### 3.4 Quadrant analysis

Analysis of JPDFs only on few grid points for the stable configuration allowed to identify mechanisms or events that contribute significantly to the production of momentum and heat fluxes. The relative contribution of these different events at the correlations  $\langle u'v' \rangle$  and  $\langle v'\theta' \rangle$  is presented in Figure 5, by quadrant analysis, for the stable and unstable configurations and for all the grid points in the transverse direction. Overall, there are two low contributions corre-

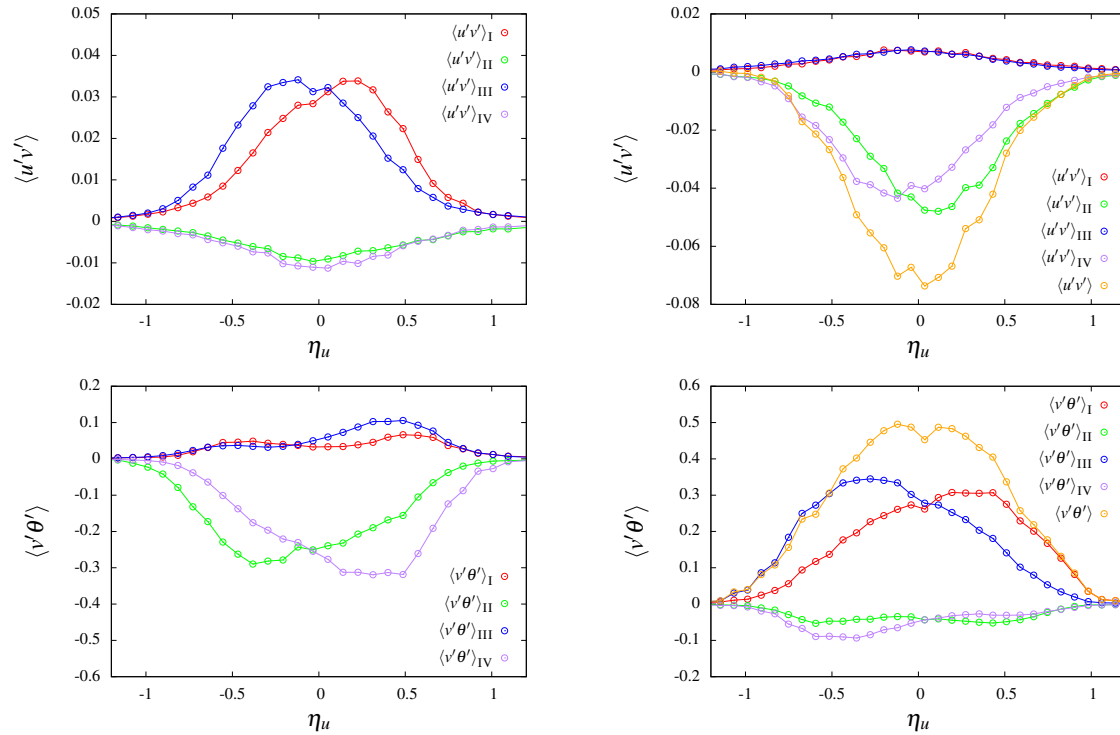


Figure 5. Quadrant analyses associated to the distributions of  $(u', v')$  and  $(v', \theta')$  through the mixing layer in the self-similar region for the stable (on the left) and the unstable (on the right) configurations.

sponding to the mixing region and two high contributions relatives to the entrainment and ejection movements. These two main contributions are bell-shaped slightly shifted always to the ejection side, meaning the dominance in intensity of the ejections on the entrainments. For the stable configuration, the contribution of ejections to  $\langle u'v' \rangle$  is the same on both sides of the axis of the mixing layer. The contribution of ejections to  $\langle v'\theta' \rangle$  is slightly higher at the low speed side compared to the same contribution to the high speed side. For the unstable configuration, the contribution of ejections to  $\langle u'v' \rangle$  and  $\langle v'\theta' \rangle$  both are slightly higher at the low speed side. These dissymmetries can partly explain the dissymmetries observed in the transverse profiles of statistical quantities, especially for quantities involving the temperature.

#### 4 Conclusions

The turbulent mixing was studied in a thermal plane turbulent mixing layer in two counter-gradient configurations with possible stabilizing or destabilizing effects of buoyancy. The simultaneous measurement of velocity and temperature by variable temperature hot wire thermoanemometry allow to identify coherent structures otherwise than with fully kinematic definition. Considering the temperature as a marker of the origin of a particle fluid, the spatial organization of the flow can be better understood. The mechanisms and events that contribute significantly to momentum and heat transverse fluxes were highlighted. These contributions were differentiated and quantified through a quadrant analysis which emphasizes the dominance of the local movements of entrainment and ejection, with a slight

dissymmetry in intensity on both sides of the axis of the mixing layer. The dissymmetry of ejections and the presence of fronts shape the transverse profiles of statistical quantities, especially involving the temperature. The buoyancy in the unstable configuration seems to reinforce the dissymmetry and affects the transport equations of turbulent kinetic energy and temperature variance.

#### ACKNOWLEDGEMENTS

We are grateful to the Region Bretagne of France for their financial support and thank our colleagues: G. Arroyo, J. Delville and M. Ndoye for their valuable advice.

#### REFERENCES

- Batt, R. G. 1977 Turbulent mixing of passive and chemically reacting species in a low speed shear layer. *J. Fluid Mech.* **22**, 93–126.
- Corrsin, S. 1947 Extended applications of hot-wire anemometer. *Rev. Sci. Instrum* **18** (7), 469–471.
- Fiedler, H. E. 1974 Transport of heat across a plane turbulent mixing layer. *Advances in Geophysics* **18**, 93–109.
- Ndoye, M. 2008 Anmometrie fil chaud temprature variable : application l'tude d'une couche de mlange anisotherme. Thèse de Ph.D., Universit de Poitiers.
- Sodjavi, K. 2013 tude experimentale de la turbulence dans une couche de mlange anisotherme. Thèse de Ph.D., Universit de Rennes 1.
- Wyganski, I. & Fiedler, H. E. 1970 the two-dimensionnal mixing region. *J. Fluid Mech.* **41**, 327–361.